CrystEngComm

Accepted Manuscript

ROYAL SOCIETY OF CHEMISTRY

www.rsc.org/crystengcomm

Cite this: DOI: 10.1039/c0xx00000x

www.rsc.org/xxxxxx

ARTICLE TYPE

Effects of Hydroxy Substitutents on Cu(II) Coordination Polymers Based on 5-Hydroxyisophthalate Derivatives and 1,4-Bis(2-methylimidazol-1-yl)benzene

Yanqing Su,[a,b] Xinxiong Li,[b] Xiaoju Li,[a,b] Hui Pan[a,b] and Ruihu Wang*[b]

Received (in XXX, XXX) Xth XXXXXXXXX 20XX, Accepted Xth XXXXXXXXX 20XX
DOI: 10.1039/b000000x

ABSTRACT

In order to systematically investigate the effects of 5-positioned substitutents in isophtahlates on the structures and properties of coordination polymers, six Cu(II) coordination polymers, $[Cu_2(bmib)(HO\text{-}ip)_2]_n$ (**1**), $[Cu_4(bmib)(OH)_2(MeO\text{-}ip)_3]_n$ (**2**), $[Cu(bmib)(MeO\text{-}ip)]_n\cdot(DMF)_{2n}\cdot(H_2O)_{2n}$ (**3**), $[Cu(bmib)_{0.5}(H_2O)(EtO\text{-}ip)]_n\cdot(DMF)_{0.5n}$ (**4**), $[Cu(bmib)(PrO\text{-}ip)]_n\cdot(H_2O)_{2.5n}$ (**5**) and $[Cu(bmib)(BnO\text{-}ip)]_n\cdot(DMF)_n$ (**6**) have been synthesized by hydrothermal reaction of 5-hydroxyisophthalate derivatives (RO-ip, R = H, Me, Et, Pr and Bn), 1,4-bis(2-methylimidazol-1-yl)benzene (bmib) and $Cu(NO_3)_2\cdot 3H_2O$. Their structures have been confirmed by single crystal X-ray diffraction analyses, IR spectra, TGA and elementary analyses. In **1**, μ_3-bridged HO-ip links dinuclear Cu(II)-carboxylate units into a 2-D layer, which is further pillared by bmib to generate a two-fold interpenetrating 3-D network. However, μ_4-bridged MeO-ip in **2** connects Cu(II) into a 3-D coordination network consisting of tetranuclear Cu(II)-carboxylate units, bmib serves as a void filler through bridging between tetranuclear units. In **3**, bis-chelating MeO-ip and bmib link Cu(II) into a 2-D layer, which is packed in an eclipsed pattern. In **4-6**, Cu(II) ions are in a distorted square-planar geometry, carboxylate ligands adopts a bis-monodentate bridging mode and connect Cu(II) ions into a charge-neutral chain. A pair of such chains in **4** is pillared by bmib to form a pillared-bichain structure, while bmib in **5** and **6** bridges the adjacent chains, resulting in the formation of different 2-D layers. The packing of 2-D layers in **5** and **6** generates 1-D channels containing guest molecules, which are confirmed by their TGA analyses. The temperature-dependent magnetic analyses show dinuclear and tetranuclear Cu(II) units make up basic magnetic unit of **1** and **2,** respectively, and they show an antiferromagnetic interaction.

INTRODUCTION

Metal-organic coordination polymers have been attracted extensive attentions in supramolecular chemistry and crystal engineering due to their fascinating structures and various potential applications, such as adsorption, separation, sensor and catalysis.[1-4] The deliberate selection of organic ligands containing appropriate coordination groups plays a crucial role in the formation of the desirable structures. In the context, the aromatic di- or multi-carboxylate ligands have been extensively employed due to their rich coordination modes and strong coordination ability toward transition metal ions.[5-9] In addition, the negative charge of carboxylate groups may compensate the positive charge from metal ions, which mitigates the effects of counter anions on the assembly process of carboxylate ligands and metal ions. In various aromatic carboxylate ligands, 5-substituted isophthalates are one type of promising dicarboxylate ligands,[8-10] its two *V*-shaped carboxylate groups may bridge metal ions or metal clusters through versatile coordination modes similar to that of isophthalate. However, the coordination polymers based on 5-substituted isophthalates is lack of preferential structures, slight variation of substitutents may result in distinct structural topologies, even the same metal ions or metal clusters are employed in their structures.[11-14] For examples, 5-aminoisophthalate connects $Cu_2(COO)_4$ paddle-wheel building units into a cubohemioctahedral nanocage,[12] 5-ethynylisophthalate links $Cu_2(COO)_4$ into a coordination nanocage covered with alkyne groups,[13] while 5-benzyloxyisophthalate connects $Cu_2(COO)_4$ into a two-dimensional (2-D) Kagomé lattice.[14] As a result, the predictive synthesis of the preferred structures with the specific functionalities still remains a scientific challenge.

Recently, a variety of metal-organic coordination polymers have been constructed using 5-substituted isophthalates and flexible bis(imidazolyl) ligands with alkyl spacers,[15,16] they play different role in the formation of the resultant frameworks. Generally, carboxylate ligands connect metal ions into charge-neutral discrete macrocycles, one-dimensional (1-D) chains, 2-D networks, while flexible imidazolyl ligands are ready to coordinate to metal centers since the flexible nature of spacers between imidazolyl rings may allow them to freely rotate and twist in the assembly process, resulting in higher-dimensional frameworks with beautiful aesthetics and useful properties.[15-18] In comparison with these flexible ligands, rigid bridging ligands with aromatic spacers, such as 1,4-bis(imidazol-1-yl)benzene (bimb), possess bulkier steric hindrance and simple

conformations.[19,20] A few of coordination polymers based on 5-substituted isophthalates and bimb have recently been reported,[21] their structural topologies are distinct from those from flexible bis(imidazolyl) ligands. In comparison with bimb, 2-methylimidazolyl ring in 4-bis(2-methylimidazol-1-yl)benzene (bmib) possesses bulkier steric hindrance than imidazolyl ring, the replacement of bimb by bmib can produce coordination polymers with interesting structures and functions. However, to our best knowledge, metal-organic coordination polymers based on bmib have not been reported hitherto. It is known that Cu(II) ion is highly Jahn-Teller active and has versatile coordination geometries, such as square-planar, trigonal bipyramidal, square-pyramidal and octahedral geometries, which may endow coordination polymers with strong susceptibility and adaptability to reaction conditions.[22] Considering geometric features of Cu(II) ions and steric hindrance of bmib, we introduce Cu(II) ions into the systems of bmib and 5-substituted isophthalate mixed ligands. With an aim of systematically exploring the effects of 5-positioned substitutents in isophtahlates on the structures and functions of coordination polymers, herein, we report syntheses and structures of six Cu(II) coordination polymers based on 5-substituted isophthalates and bmib, $[Cu_2(bmib)(HO\text{-}ip)_2]_n$ (**1**), $[Cu_4(bmib)(OH)_2(MeO\text{-}ip)_3]_n$ (**2**), $[Cu(bmib)(MeO\text{-}ip)]_n\cdot(DMF)_{2n}\cdot(H_2O)_{2n}$ (**3**), $[Cu(bmib)_{0.5}(H_2O)(EtO\text{-}ip)]_n\cdot(DMF)_{0.5n}$ (**4**), $[Cu(bmib)(PrO\text{-}ip)]_n\cdot(H_2O)_{2.5n}$ (**5**) and $[Cu(bmib)(BnO\text{-}ip)]_n\cdot(DMF)_n$ (**6**) (HO-ip = 5-hydroxyisophthalate, MeO-ip = 5-methoxyisophthalate, EtO-ip = 5-ethoxyisophthalate, PrO-ip = 5-propoxyisophthalate and BnO-ip = 5-benyloxyisophthalate).

EXPERIMENTAL SECTION

Materials and General methods

MeO-ip, EtO-ip, PrO-ip, and BnO-ip were prepared according to literature methods,[23] other chemicals were commercially available and used as purchased. IR spectra (KBr pellets) were recorded on a Magna 750 FT-IR spectrophotometer in the range of 400-4000 cm^{-1}. ^1H and ^{13}C NMR spectra were recorded on a Bruker AVANCE III NMR spectrometer at 400 and 100 MHz, respectively, using tetramethylsilane (TMS) as an internal standard. Powder X-ray diffraction data (PXRD) were recorded on a PANaytical X'pert pro X-ray diffractometer with graphite-monochromatized Cu-Kα radiation (λ = 1.542 Å). The magnetic susceptibility data were collected on a Quantum Design MPMS model 6000 magnetometer in the temperature range of 2-300 K. Thermogravemetric analyses (TGA) were carried out on a NETSCHZ STA 449C thermoanalyzer under N_2 at a heating rate of 10 ^oC/min. C, H, and N elemental analyses were determined on an EA1110 CHNS-0 CE element analyzer.

X-Ray Crystallography: Single crystals of complexes **1-6** were mounted on a glass fiber for X-ray diffraction analysis. Data sets were collected on a Rigaku AFC7R equipped with a graphite-monochromated Mo-Kα radiation (λ = 0.71073 Å) from a rotating anode generator at 293 K. Intensities were corrected for LP factors and empirical absorption using the ψ scan technique. The structures were solved by direct methods and refined on F^2 with full-matrix least-squares techniques using the SHELX-97 program package.[24] All non-hydrogen atoms were refined anisotropically. The hydrogen atom of hydroxide in complex **2** was located from the difference Fourier map and refined isotropically. The positions of other hydrogen atoms were generated geometrically (C-H bond fixed at 0.96 Å), assigned isotropic thermal parameters, and allowed to ride on their parent carbon atoms before the final cycle of refinement. Crystal data as well as the details of data collection and refinement for complexes **1-6** are summarized in Table 1. The selected bond distances and bond angles are given in Table S1 in supporting information. Crystallographic data of **1-6** have been deposited in the Cambridge Crystallographic Data Centre as supplementary publication with CCDC number: 1044062-1044066 and 1044091.

Synthesis of bmib: A Schlenk flask was charged with 1,4-dibromobenzene (8.0 g, 0.034 mol), 2-methyl-1H-imidazole (28 g, 0.34 mol), K_2CO_3 (47 g, 0.34 mol) and $CuSO_4\cdot5H_2O$ (2.0 g, 0.008 mol). The mixture was degassed through three freeze-pump-thaw cycles using liquid nitrogen, and then heated at 200 ^oC for 60 h. After water (100 mL) was added to the reaction system, the resultant mixture was extracted three times using dichloromethane. The organic layer was washed with brine and water, and dried over $MgSO_4$. After the removal of organic solvents under the reduced pressure, the residue was recrystallized in EtOH to provide a pale yellow solid. Yield: 4.5 g (55 %). ^1H NMR ($CDCl_3$): δ 7.45 (s, 4H), 7.08 (d, J = 8.1 Hz, 4H), 2.45 (s, 6H). ^{13}C NMR ($CDCl_3$): δ 137.7, 133.1, 128.3, 127.61, 121.0, 14.0.

Synthesis of $[Cu_2(bmib)(HO\text{-}ip)_2]_n$ (1): A mixture of $Cu(NO_3)_2\cdot3H_2O$ (0.20 mmol, 0.048 g), HO-ip (0.10 mmol,0.018 g), bmib (0.10 mmol, 0.024 g) and HCl (1.0 $mol\cdot L^{-1}$, 0.2 mL) in DMF (5 mL) and H_2O (5 mL) was stirred for 5 min. The mixture was transferred into a heat-resistant glass bottle (20 mL), and was heated at 100 ^oC, turquoise crystals were obtained in 3 days. Yield: 0.017 g (47% based on HO-ip). IR (KBr pellet, cm^{-1}): 3304 (m), 3134 (w), 3073 (vw), 1796 (vw), 1623 (m), 1574 (vs), 1522 (s), 1489 (m), 1421 (s), 1417 (s), 1371 (vs), 1275 (s), 1210 (m), 1148 (m), 1103 (vw), 1007 (w), 980 (w), 890 (w), 853 (w), 773 (s), 730 (s), 667 (m), 571 (w), 491 (w). Elemental analyses calcd (%) for $C_{30}H_{22}N_4O_{10}Cu_2$ (725.60): C, 49.66; H, 3.06; N, 7.72. Found: C, 49.22; H, 3.16; N, 7.89.

Synthesis of $[Cu_4(bmib)(OH)_2(MeO\text{-}ip)_3]_n$ (2): A mixture of $Cu(NO_3)_2\cdot3H_2O$ (0.20 mmol, 0.048 g), MeO-ip (0.10 mmol, 0.020 g), bmib (0.10 mmol, 0.024 g) and HCl (1.0 $mol\cdot L^{-1}$, 0.2 mL) in DMF (5 mL) and H_2O (5mL) was stirred for 5 min. The mixture was transferred into a heat-resistant glass bottle (20 mL), and was heated at 100 ^oC, turquoise crystals were obtained after 3 days. Yield: 0.013 g (35% based on MeO-ip). IR (KBr pellet, cm^{-1}): 3410 (m), 2960 (vw), 2834 (vw), 1626 (m), 1563 (s), 1510 (m), 1438 (m), 1366 (vs), 1321 (m), 1263 (m), 1125 (w), 1053 (w), 1003 (w), 919 (vw), 883 (vw), 851 (w), 780 (m), 720 (m), 672 (vw), 516 (w). Elemental analyses calcd (%) for $C_{41}H_{34}N_4O_{17}Cu_4$ (1108.88): C, 44.41; H, 3.09; N, 5.05. Found: C, 44.52; H, 3.16; N, 5.23.

Synthesis of $[Cu(bmib)(MeO\text{-}ip)]_n\cdot(DMF)_{2n}\cdot(H_2O)_{2n}$ (3): A mixture of $Cu(NO_3)_2\cdot3H_2O$ (0.20 mmol, 0.048 g), MeO-ip (0.10 mmol, 0.020 g), bmib (0.1 mmol, 0.024 g) and HCl (1.0 $mol\cdot L^{-1}$, 0.1 mL) in DMF (5 mL) and H_2O (5 mL) was stirred for 5 min. The mixture was transferred into a heat-resistant glass bottle (20

mL), and was heated at 100 °C, blue crystals were obtained after 3 days. Yield: 0.010 g (32% based on MeO-ip). IR (KBr pellet, cm^{-1}): 3452 (s), 3125 (w), 3083 (vw), 2933 (vw), 2853 (vw), 1670 (vs), 1567 (s), 1525 (s), 1394 (s), 1347 (s), 1310 (m), 1255 (w), 1169 (w), 1123 (w), 1092 (w), 1052 (w), 1011 (w), 917 (vw), 847 (w), 777 (m), 735 (m), 665 (w), 571 (w), 515 (w). Elemental analyses calcd (%) for $C_{29}H_{29}N_6O_9Cu$ (669.12): C, 52.05; H, 4.37; N, 12.56. Found: C, 51.67; H, 5.50; N, 12.38.

Synthesis of $[Cu(bmib)_{0.5}(H_2O)(EtO\text{-}ip)]_n\cdot(DMF)_{0.5n}$ (4): A mixture of $Cu(NO_3)_2\cdot 3H_2O$ (0.20 mmol, 0.048 g), EtO-ip (0.10 mmol, 0.021 g), bmib (0.10 mmol, 0.024 g) and HCl (1.0 $mol\cdot L^{-1}$, 0.1 mL) in DMF (5 mL) and H_2O (5 mL) was stirred for 5 min. The mixture was transferred into a heat-resistant glass bottle (20 mL), and was heated at 100 °C, blue crystals were obtained after 3 days. Yield: 0.020 g (45% based on EtO-ip). IR (KBr pellet, cm^{-1}): 3252 (w), 3130 (w), 2982 (vw), 1663 (m),1617 (m), 1578 (s), 1518 (m), 1447 (m), 1413 (m), 1363 (vs), 1312 (m), 1257 (w), 1161 (w), 1054 (w), 852 (vw), 773 (w), 722 (w), 670 (vw), 569 (vw), 515 (vw), 478 (vw), 423 (vw). Elemental analyses calcd (%) for $C_{18.5}H_{20.5}N_{2.5}O_{6.5}Cu$ (445.42): C, 49.88; H, 4.64; N, 7.86. Found: C, 49.98; H, 4.60; N, 7.93.

Synthesis of $[Cu(bmib)(PrO\text{-}ip)]_n\cdot(H_2O)_{2.5n}$ (5): A mixture of $Cu(NO_3)_2\cdot 3H_2O$ (0.10 mmol, 0.024 g), PrO-ip (0.10 mmol, 0.022 g), bmib (0.10 mmol, 0.024 g) and HCl (1.0 $mol\cdot L^{-1}$, 0.1 mL), in DMF (5 mL) and H_2O (5 mL) was stirred for 5 min. The mixture was transferred into a heat-resistant glass bottle (20 mL), and was heated at 100 °C, blue crystals were obtained after 3 days. Yield: 0.025 g (43% based on PrO-ip). IR (KBr pellet, cm^{-1}): 3123 (w), 2968 (vw), 1618 (w), 1574 (s), 1519 (m), 1445 (w), 1360 (vs), 1310 (m), 1262 (m), 1157 (w), 1115 (w), 1046 (w), 1011 (w), 905 (vw), 854 (w), 806 (w), 777 (m), 738 (m), 673 (w), 504 (w). Elemental analyses calcd (%) for $C_{25}H_{30}N_4O_8Cu$ (569.07): C, 52.77; H, 5.14; N, 9.85. Found: C, 52.49; H, 5.19; N, 9.97.

Synthesis of Crystal structure of $[Cu(bmib)(BnO\text{-}ip)]_n\cdot(DMF)_n$ (6): A mixture of $Cu(NO_3)_2\cdot 3H_2O$ (0.10 mmol, 0.024 g), BnO-ip (0.10 mmol, 0.027 g), bmib (0.10 mmol, 0.024 g) and HCl (1.0 $mol\cdot L^{-1}$, 0.1 mL) in DMF (5 mL) and H_2O (5 mL) was stirred for 5 min. The mixture was transferred into a heat-resistant glass bottle (20 mL), and was heated at 100 °C, blue crystals were obtained after 3 days. Yield: 0.015 g (47% based on BnO-ip). IR (KBr pellet, cm^{-1}): 3657 (vw), 3120 (w), 2913 (vw), 2868 (vw), 1616 (m), 1576 (s), 1522 (s), 1455 (m), 1415 (m), 1390 (m), 1336 (vs), 1270 (m), 1258 (m), 1175 (w), 1159 (w), 1114 (m), 1039 (w), 1013 (w), 919 (vw), 887 (vw), 844 (w), 795 (m), 775 (m), 754 (m), 730 (s), 701 (w), 677 (w), 572 (w), 502 (w), 457 (vw), 421 (vw). Elemental analyses calcd (%) $C_{32}H_{31}N_5O_6Cu$ (645.16): C, 59.57; H, 4.84; N, 10.86. Found: C, 59.83; H, 4.79; N, 10.87.

Table 1. Crystal data and structure refinement results for complexes **1-6.**

	1	**2**	**3**	**4**	**5**	**6**
Empirical formula	$C_{15}H_{11}CuN_2O_5$	$C_{20.5}H_{17}Cu_2N_2O_{8.5}$	$C_{14.5}H_{14.5}Cu_{0.5}N_3O_{4.5}$	$C_{34}H_{34}Cu_2N_4O_{12}$	$C_{25}H_{29}CuN_4O_{7.5}$	$C_{16}H_{15.5}Cu_{0.5}N_{2.5}O_3$
Formula weight	362.8	554.44	334.56	817.73	569.06	645.16
Crystal system	Monoclinic	Monoclinic	Orthorhombic	Monoclinic	Triclinic	Orthorhombic
Space group	*P*2(1)/*c*	*C*2/*c*	*Pbcn*	*C*2/*c*	*P*-1	*P*nma
a (Å)	8.7922(6)	26.424(14)	13.5914(6)	23.182(11)	7.751(2)	12.725(5)
b (Å)	14.9186(8)	9.529(4)	12.6315(7)	12.610(5)	12.916(3)	18.008(8)
c (Å)	13.419(1)	19.889(11)	18.4809(9)	17.333(8)	14.603(4)	13.521(6)
α (°)	90	90	90	90	83.875(6)	90
β (°)	120.130(5)	124.468(8)	90	130.001(7)	88.192(7)	90
γ (°)	90	90	90	90	74.126(6)	90
V (Å^3)	1522.4(2)	4129(4)	3172.8(3)	3881(3)	1398.1(6)	3098(2)
Z	4	8	4	4	2	8
F(000)	736	2240	1384	1680	592	1340
ρ_{calcd}(g cm^{-3})	1.583	1.784	1.401	1.399	1.352	1.383
μ(mm^{-1})	1.461	2.116	0.749	1.158	0.831	0.757
Reflections collected	12583	15677	25129	14575	11757	21554
Unique reflections	3465	4732	3614	4308	6181	3667
Parameters	209	314	222	237	349	237
R_{int}	0.0316	0.0307	0.0239	0.0243	0.0407	0.0318
S on F^2	1.088	1.073	1.128	1.058	1.062	1.074
R_1 (I>2σ(I))[a]	0.0372	0.0350	0.0561	0.0304	0.0596	0.0483
wR_2 (I>2σ(I))[b]	0.0897	0.0876	0.1514	0.0812	0.1708	0.1104
R_1 (all data)[a]	0.0411	0.0421	0.0598	0.0335	0.0876	0.0599
wR_2 (all data)[b]	0.0922	0.0922	0.1550	0.0826	0.1920	0.1191
$\Delta\rho_{max}$ and $_{min}$ [e·Å^{-3}]	0.495 and -0.503	0.507 and -0.433	0.583 and -0.471	0.281 and -0.233	0.920 and -0.609	0.330 and -0.315

[a] $R_1 = \sum||F_o| - |F_c||/\sum|F_o|$. [b] $wR_2 = [\sum w(F_o^2 - F_c^2)^2/\sum w(F_o^2)^2]^{1/2}$

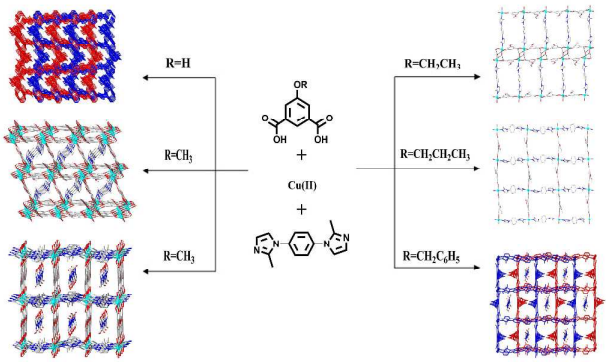

Scheme 1 The summary of crystal structures in complexes **1-6**.

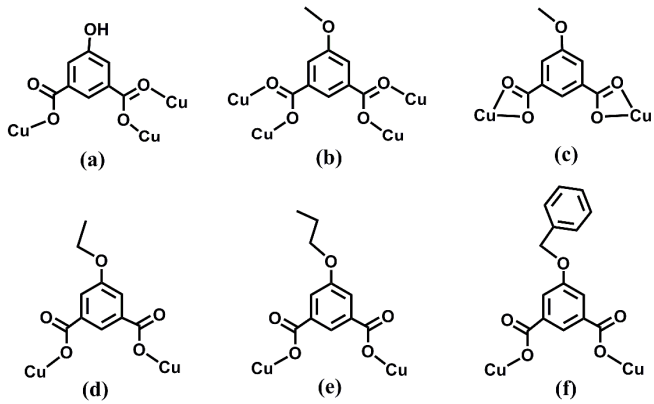

Scheme 2 The coordination modes of carboxylate ligands used in this work.

RESULTS AND DISCUSSION

Synthesis

It is known that 5-positioned substitutents of isophthalate derivatives have important effects on the structures and properties of metal-organic coordination polymers, even they do not take part in coordination with metal ions.[9,16] The assembly of transition metal ions with HO-ip and flexible *exo*-bidentate nitrogen-containing ligands, such as 1,4-bis(imidazol-1-yl)butane and 1,2-di-(4-pyridyl)ethane, generated a series of two-fold interpenetrating pillared-layer structures, in which strong hydrogen bonds between hydroxy and carboxylate oxygen atoms of different HO-ip probably play important roles in the formation of two-fold interpenetrating frameworks.[15, 25] The replacement of hydroxy of HO-ip by alkyloxo groups may prevent the formation of these hydrogen bonds, resulting in the coordination polymers with different structures and properties.[16] Therefore, the systematical investigation for the effects of alkyloxo substitutents in 5-hydroxyisophthalate derivatives will be beneficial for design and synthesis of the desirable coordination polymers owing to the simple synthetic procedures of 5-alkyloxyisophthalates. In this work, rigid bmib was chosen as auxiliary ligands. As shown in Scheme 1, hydrothermal reaction of HO-ip, bmib and $Cu(NO_3)\cdot 3H_2O$ gave rise to a two-fold interpenetrating 3-D network. The structural framework is similar to those from HO-ip and flexible 1,4-bis(imidazol-1-yl)butane,[15a] which further suggesting the crucial role of directional hydrogen bonds from hydroxy of HO-ip in the assembly process. Replacement of HO-ip by MeO-ip generated a 3-D coordination network consisting of tetranuclear Cu(II)-carboxylate units and a 3-D supramolecular network containing 1-D channels, respectively, depending on pH values of the reaction systems. Further extension of 5-positioned substitutents from MeO- to EtO- resulted in the formation of a 2-D supramolecular network containing pillared-bichain structure, when bulkier PrO- and BnO- were used as substitutents, 2-D layer containing rectangular cavities were formed. An obvious substituent effect of alkyloxo groups in isophtahalte derivatives has been displayed since bmib in complexes **1-6** just adopts an *anti* conformation (Scheme S1).

Structural description

Crystal structure of $[Cu_2(HO\text{-}ip)_2(bmib)]_n$ (1): Single crystal X-ray diffraction analysis shows that complex **1** crystallizes in the monoclinic space group $P2(1)/c$, and is a two-fold interpenetrating 3-D network consisting of dinuclear Cu(II)-carboxylate units. The asymmetric unit contains one Cu(II), one HO-ip and half of bmib. As shown in Figure 1a, Cu1 is in a highly distorted square-planar geometry if neglecting Cu1-O3A distance of 2.680 Å, it is coordinated by one 2-methylimidazolyl nitrogen atom and three carboxylate oxygen atoms from different HO-ip. The Cu1-N/O bond distances vary from 1.9488(15) to 1.9667(16) Å, and *cis*-angles range from 87.37(7) to 97.11(7)°. The mean deviation of Cu1 from the plane determined by four equatorial atoms (N1, O1, O2B and O4A) is 0.0214 Å. Cu1 and Cu1B are equivalently bridged by two μ_2,η^2-carboxylate from different HO-ip to form a binuclear Cu(II)-dicarboxylate unit. Cu···Cu distance in the dinuclear unit is 2.8538(5) Å, which is longer than that in paddle-wheel dinuclear Cu(II) units.[26] HO-ip bridges three Cu(II) through μ_2,η^2-carboxylate and monodentate carboxylate (Scheme 2a). As shown in Figure S1, HO-ip links two adjacent dinuclear Cu(II) units into a charge-neutral $[Cu_2(HO\text{-}ip)_2]_n$ layer containing square-shaped cavities, the dimensions of each cavity are *ca.* 9.199 × 9.199 $Å^2$ based on the nearest Cu···Cu separations across HO-ip. bmib adopts an *anti* conformation to bridge two Cu(II) ions (Scheme S1), Cu···Cu distance across bmib is 13.499 Å[3]. Two 2-methylimidazoly rings in bmib are parallel to each other owing to center symmetry, the twisting angles between 2-methylimidazolyl ring and the central phenyl ring is 71.102(3)°. The *exo*-bidentate bmib serves as a pillar between two adjacent layers to afford a 3-D open framework containing large cavities (Figure 1b). The large void in the 3-D network results in the formation of a two-fold interpenetrating framework owing to the absence of guest molecules to fill the void. (Figure S2). As expected, the hydroxy of HO-ip is not involved in coordination, and forms strong hydrogen bonds with uncoordinated carboxylate oxygen atom from the other 3-D network [O(5)-H(5)···O3^{i} 2.771(3) Å, symmetry code: (i) x+1, -y+1/2, z+1/2]. The nearest Cu···Cu separation between two adjacent interpenetrating 3-D networks is 6.711 Å. Topological analysis was applied to have a better insight into the 3-D structure. Taking the center of each binuclear Cu(II)-carboxylate unit as one node, each dinuclear unit becomes a 6-connected node. HO-ip and bmib may serve as two independent two-connected vertex that link two adjacent nodes. Their interlinkage generates a 6-connected α-Po topology (Figure 1c).

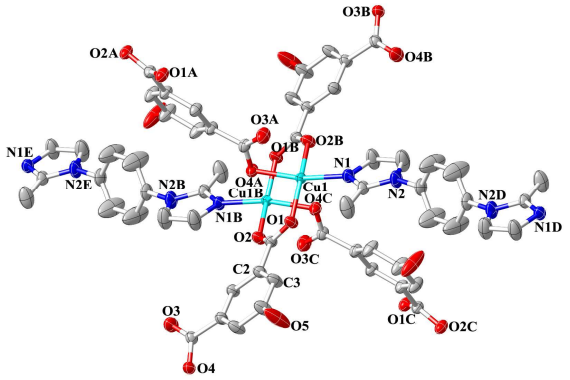

Figure 1a View of the coordination environment of Cu(II) with thermal ellipsoids at 50% probability in complex **1**.

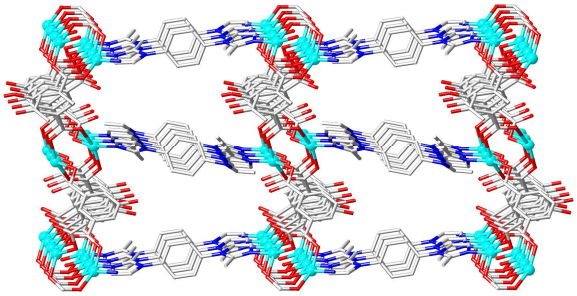

Figure 1b View of 3-D open framework in complex **1**.

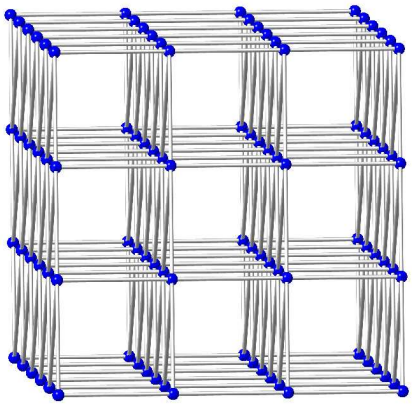

Figure 1c Schematic representation of 6-connected α-Po topology.

Crystal structure of $[Cu_4(bmib)(OH)_2(MeO\text{-}ip)_3]_n$ (2): Complex **2** crystallizes in the monoclinic space group *C*2/*c*, and is a 3-D coordination network consisting of tetranuclear Cu(II)-carboxylate units, while the coordination polymers based on MeO-ip consist of paddle-wheel dinuclear Cu(II)-carboxylate units,[16b] suggesting the introduction of bmib has an important effect on the structures of coordination polymers. As shown in Figure 2a, Cu1 and Cu2 are five-coordianted, but they display different coordination environments. Cu1 takes a distorted square-pyramidal geometry. The equatorial plane is defined by two μ_2,η^2-carboxylate oxygen atoms from different MeO-ip (O1 and O3E), one μ_3-OH (O9) and one 2-methylimidazolyl nitrogen atom (N1). The apical position is occupied by one μ_2,η^2-carboxylate oxygen atom (O6). The Cu1-O6 bond distance is 2.245(2) Å, which is much longer than Cu1-N/O bond distances from 1.934(2) to 2.045(2) Å in the equatorial plane. Cu2 is coordinated by three μ_2,η^2-carboxylate oxygen atoms and two μ_3-OH in a distorted trigonal bipyramidal geometry. The apical positions are occupied by one μ_3-OH and one carboxylate oxygen atom with the O4F-Cu2-O9 bond angle being 179.14(8)°, the remaining three oxygen atoms (O2, O7A and O9A) comprise the equatorial plane. Interestingly, Cu2 and symmetry-related Cu2A are bridged by a pair of μ_3-OH to form a dinuclear subunit. The Cu2···Cu2A distance in the subunit is 3.046(1) Å. The dinuclear subunit is further connected to Cu1 and Cu1A by two μ_3-OH and six μ_2,η^2-carboxylate from different MeO-ip to form a tetranuclear Cu(II) unit. Cu1···Cu2 and Cu1···Cu2A distances separated by one μ_2,η^2-carboxylate and two μ_2,η^2-carboxylate are 3.247 and 3.450 Å, respectively. Cu1···Cu1A distance in the tetranuclear unit is 5.969 Å. MeO-ip serves as a μ_4-bridge through two μ_2,η^2-carboxylate groups (Scheme 2b). MeO-ip links two adjacent tetranuclear Cu(II) units into a 3-D network containing square-shaped cavities (Figure 2b). The *anti*-conformationed bmib serves as a filler of the cavities through bridging two Cu1 from different tetranuclear units. Two 2-methylimidazoly rings of bmib are parallel to each other owing to center symmetry, the twisting angles between 2-methylimidazolyl ring and the central phenyl ring is 40.038(7)°. Cu(II)···Cu(II) separation across bmib is 13.529 Å, which is close to that in **1**. Better insight into such elegant framework was performed by topological analysis. If taking the center of tetranuclear Cu(II) unit as a node, each tetranuclear unit becomes an eight-connected node, MeO-ip and bimb can be regarded as independent two-connected vertexes. The interlinkage of eight nodes with six MeO-ip and two bimb generates a new topology with Schläfli symbol of $\{4^{12}\cdot5^8\cdot6^7\cdot7\}$.

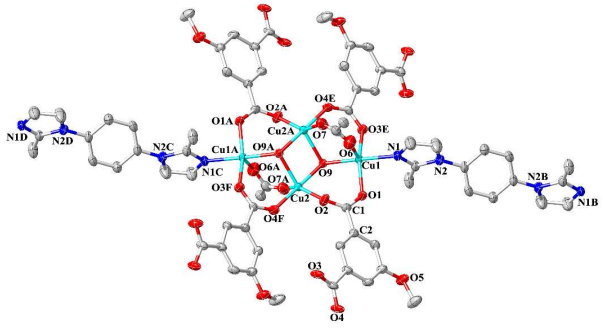

Figure 2a View of the coordination environment of Cu(II) with thermal ellipsoids at 50% probability in complex **2**.

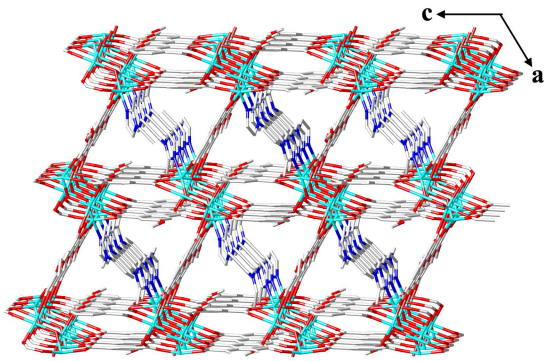

Figure 2b View of 3-D network in complex **2**.

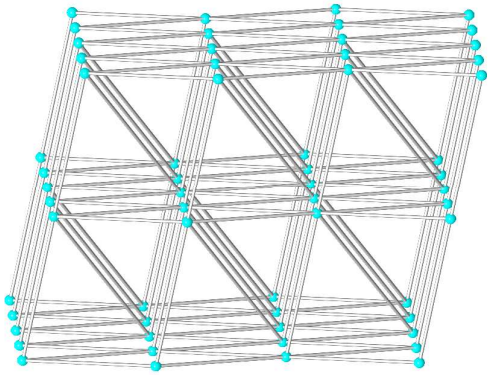

Figure 2c View of eight-connected topology in complex **2**.

Crystal structure of $[Cu(bmib)(MeO\text{-}ip)]_n\cdot(DMF)_{2n}\cdot(H_2O)_{2n}$ (3): Complex **3** crystallizes in the orthorhombic space group *Pbcn*, and is a 2-D layer. As shown in Figure 3a, Cu1 is in a slightly distorted octahedral geometry, and is coordinated by four oxygen atoms of two chelating carboxylate from different MeO-ip, and two 2-methylimidazolyl nitrogen atoms from different bmib. Two nitrogen atoms occupy the axial positions with the Cu1-N1 bond distances being 1.981(2) Å. Four oxygen atoms comprise the equatorial plane, and Cu1 is in the center of the plane. The Cu1-O1 and Cu1-O2 bond distances are 2.084(2) and 2.412(2) Å, which is longer than the Cu1-N1 bond distance, suggesting a compressed octahedron. MeO-ip bridges two Cu(II) ions through two chelating carboxylate groups (Scheme 2c). MeO-ip and *anti*-conformationed bmib link Cu(II) into a charge-neutral 2-D layer containing rectangular-shape cavities (Figure 3b), in which MeO- group alternately points toward the opposite directions. Interestingly, water molecules locate insides cavum of two adjacent layers and form interlayer hydrogen bonds with carboxylate oxygen atoms and the adjacent water molecules [O1W-H···O1 2.887 Å, O1W-H···O1W^{i} 2.881 Å, symmetry code: (i) 1/2-*x*, *y*-1/2, *z*] (Figure S3). The most striking structure feature in **3** is such 2-D layers are packed in an eclipsed pattern along the *b* axis, resulting in the formation of 1-D channels (Figure 3c), the sizes of the channels are 9.240 x 13.591 Å based on Cu···Cu separations. DMF molecules reside in the cavities to fill with its void space. PLATON analysis shows that the accessible void volume is 39.2% of per unit cell volume after the removal of water and DMF molecules.

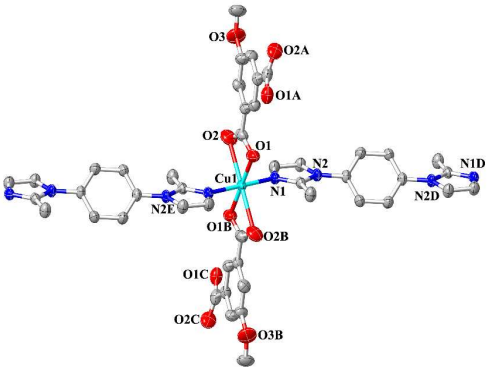

Figure 3a View of the coordination environment of Cu(II) with thermal ellipsoids at 50% probability in complex **3**.

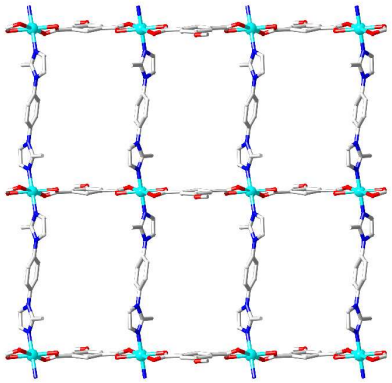

Figure 3b View of 2-D layer in complex **3**.

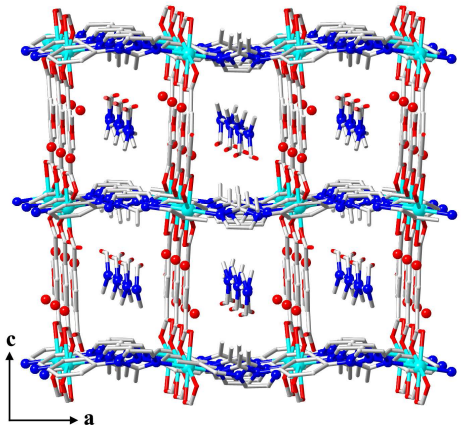

Figure 3c View of packing diagram with 1-D channels along the *b* axis in complex **3**.

Crystal structure of $[Cu(bmib)_{0.5}(H_2O)(EtO\text{-}ip)]_n\cdot(DMF)_{0.5n}$ (4): Complex **4** crystallizes in the monoclinic space group *C*2/*c*, and is a pillared-bichain structure. As shown in Figure 4a, Cu1 is in a square-planar geometry, and is coordinated by two carboxylate oxygen atoms from different EtO-ip, one 2-methylimidazolyl nitrogen atom and one water molecule. The Cu1-N/O bond distances fall in the range of 1.9576(14)-1.9893(18) Å, and *cis*-angles range from 89.40(6) to 90.81(6)°. EtO-ip acts as a bis-monodentate ligand (Scheme 2d), two carboxylate groups are highly twisted with the central phenyl ring with the dihedral angles between carboxylate and phenyl ring being 23.179(4) and 14.319(3)°, respectively. EtO-ip connects Cu(II) ions into a charge-neutral $[Cu(EtO\text{-}ip)]_n$ chain. Notably, a pair of such chains are pillared by bmib to form a pillared-bichain structure containing rectangular cavities (Figure S4), the sizes of each cavity are 9.322 x 13.648 Å^2 based on Cu···Cu separations across EtO-ip and bmib, respectively, which are very close to that in **3**. Two 2-methylimidazolyl rings in *anti*-conformationed bmib are parallel to each other owing to center symmetry, the dihedral angle between 2-methylimidazolyl ring and the central phenyl ring is 44.499(15)°. To our knowledge, the pillared-bichain complex is unprecedented hitherto in Cu(II) coordination polymers. Interestingly, the neighboring bichains are connected with each other through strong hydrogen bonds between coordinated water molecules and uncoordinated carboxylate oxygen atoms [O1W-H6A···O1^{i} 2.657(2) Å, O1W-H6B···O4^{ii}

2.615 Å, symmetry code: (i) -*x*+1/2, -*y*+1/2, -*z*; (ii) -*x*, *y*, -*z*-1/2], resulting in the formation of a 2-D supramolecular network (Figure 4b). Such supramolecular networks are further packed in an ABAB mode, generating 1-D channels along the *c* axis (Figure 4c). To preclude large void space, the channels are inserted by EtO- group of EtO-ip, the remaining space is further filled by DMF molecules, which are difficult to be defined by X-ray analysis owing to their high disorder.

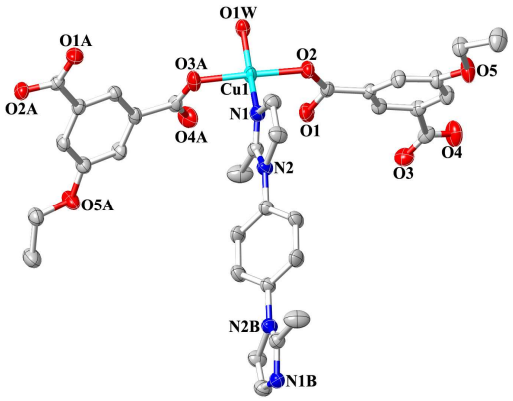

Figure 4a View of the coordination environment of Cu(II) with thermal ellipsoids at 50% probability in complex **4**.

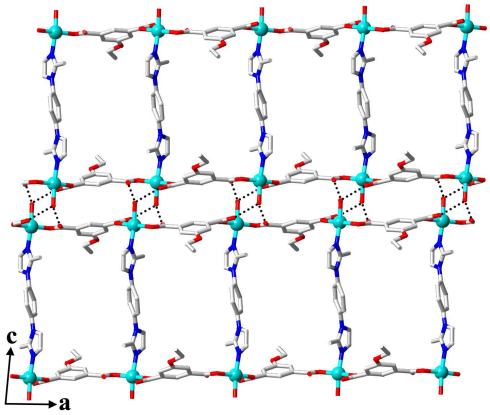

Figure 4b View of 2-D supramolecular layer along the *b* axis in **4**.

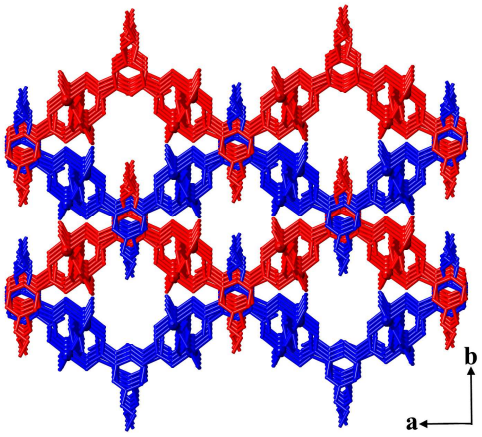

Figure 4c View of packing diagram along the *c* axis in complex **4**.

Crystal structure of $[Cu(bmib)(PrO\text{-}ip)]_n\cdot(H_2O)_{2.5n}$ (5): Complex **5** crystallzies in the triclinic space group *P*-1. As shown in Figure 5a, Cu1 and Cu2 take a distorted square-planar geometry, and are coordinated by two carboxylate oxygen atoms from different PrO-ip and two 2-methylimidazolyl nitrogen atoms from diifernet bmib. The Cu-N/O bond distances are in the range from 1.953(2) to 2.006(3) Å, and *cis*-angles are in the range from 87.69(12) to 92.31(12)°. Similar to EtO-ip in complex **4**, PrO-ip shows a bis-monodentate bridging mode (Scheme 2e), the twisting angles between two carboxylate groups and the central phenyl rings are 10.123 and 15.743°, respectively. bmib also adopts an *anti* conformation, two 2-methylimidazolyl rings are drastically twisted with the central phenyl ring, the dihedral angles between 2-methylimdazolyl and phenyl ring are 59.122(2) and 67.661(6)°, respectively. PrO-ip links two adjacent Cu(II) ions into a 1-D charge-neutral chain, subsequent bridging by bmib results in the formation of 2-D layer containing rectangular cavities (Figure 5b). The sizes of each cavity are 10.229 x 13.579 $Å^2$ based on Cu···Cu separations across EtO-ip and bmib, respectively, which are comparable with that in **3**. EtO- group of EtO-ip is threaded into the lateral void of the adjacent layers in an offset mode in order to stabilize the structural framework (Figure S5). When viewed along the *a* axis, the framework contains 1-D channels, in which water molecules are filled (Figure 5c). The accessible void volume is 18.9 % of per unit cell volume after the removal of water molecules as calculated by PLATON.

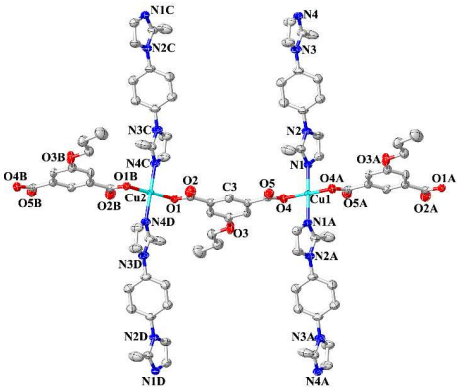

Figure 5a View of the coordination environment of Cu(II) with thermal ellipsoids at 50% probability in complex **5**.

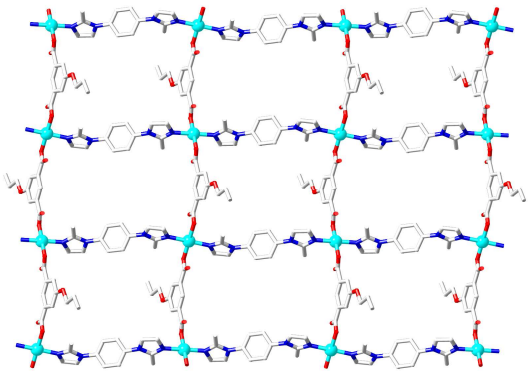

Figure 5b View of 2-D layer in complex **5**.

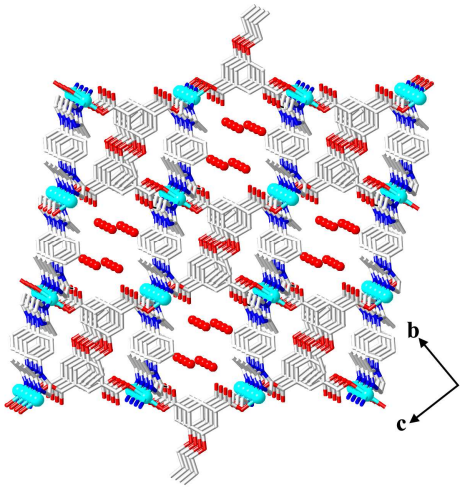

Figure 5c View of packing diagram along the *a* axis in **5**.

Crystal structure of $[Cu(bmib)(BnO\text{-}ip)]_n \cdot (DMF)_n$ (6): Complex **6** crystallizes in the orthorhombic space group *P*nma, and is a 2-D layer, which is much different from 2-D Kagomé lattice based on BnO-ip owing to the introduction of bmib. As shown in Figure 6a, Cu1 takes a distorted square-planar geometry, it is coordinated by two carboxylate oxygen atoms from different BnO-ip and two 2-methylimidazolyl nitrogen atoms from different bmib. Cu1 resides in the center of the basal plane. The Cu1-N1 and Cu1-O1 bond distances are 1.978(2) and 2.004(2) Å, respectively. Similar to EtO-ip in **4** and PrO-ip in **5**, BnO-ip acts as a bis-monodentate ligand (Scheme 2f), benzyl ring is almost perpendicular to the central phenyl ring with the dihedral angle between them being 74.487(8)º. BnO-ip and bmib connects Cu(II) ions into a 2-D layer containing rectangular cavities (Figure 6b). The sizes of each cavity are 9.004 x 13.521 $Å^2$ based on Cu···Cu separations across BnO-ip and bmib, respectively. Benzyl group in BnO-ip locates alternatively two lateral sides of 2-D layer. Interestingly, such layers are packed in an ABAB mode, benzyl groups are interpenetrated into the cavities of the neighboring layers (Figure 6c), DMF molecules lie in the cavities to further fill with large void space (Figure 6d). PLATON analysis shows that the accessible void volume is 17.7 % of per unit cell volume after the removal of DMF molecules.

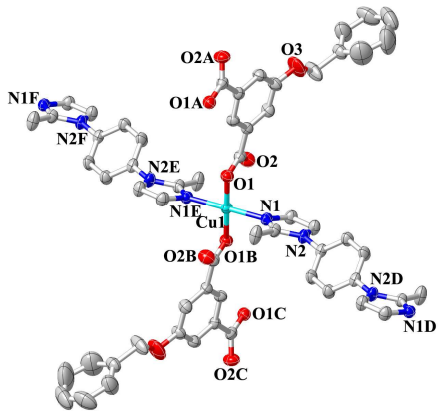

Figure 6a View of the coordination environment of Cu(II) with thermal ellipsoids at 50% probability in complex **6**.

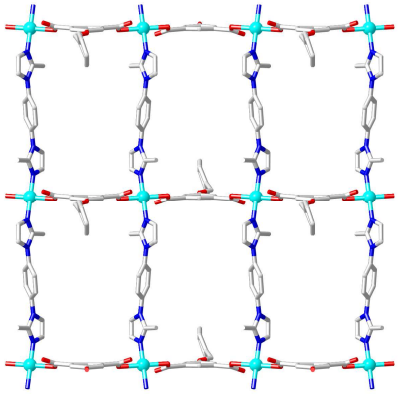

Figure 6b View of 2-D layer along the *a* axis in complex **6**.

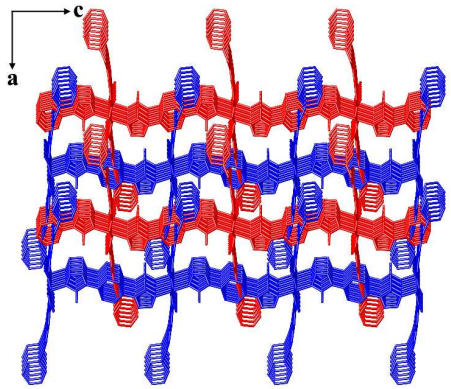

Figure 6c View of 2-D layer along the *b* axis in complex **6**.

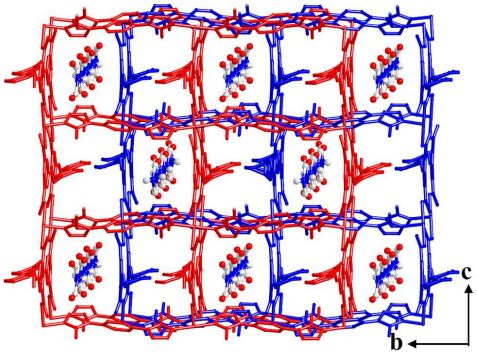

Figure 6d View of packing diagram of 2-D layers with DMF molecules along the *a* axis in complex **6**.

Thermal properties

Thermal stability of complexes **1-6** was investigated using as-synthesized crystalline samples. TGA curves in Figure S6 show that complexes **1** and **2** are stable before 280 and 250 °C, respectively. For **3**, the continuous weight loss of 27.37 % before 150 °C corresponds to the removal of lattice water and DMF molecules (calcd 27.23%), subsequent collapse of structrual framework is obersved. The weight loss of 12.30 % before 180 °C in **4** is attributed to the loss of water and DMF molecules

(calcd 12.25 %). The structural frameworks of **3** and **4** start to collapse after 250 and 280 °C, respectively. For **5** and **6**, the weight losses of 6.83 and 11.30 % occur before 150 and 190 °C, respectively, corresponding to the release of water (calcd 6.23%) and DMF (calcd 13.50%), respectively. **5** and **6** are stable up to 260 and 280 °C, respectively.

PXRD patterns

In order to check purity of these complexes, PXRD of **1**-**6** were measured at room temperature. As shown in Figure S7, PXRD patterns for the as-synthesized bulk materials match well with the simulated ones from single crystal X-ray diffraction analysis, suggesting good phase purity and homogeneity of these complexes. The differences in intensity may be ascribed to preferable orientation of the crystalline powder samples.

Bond valence analysis

Since complexes **1** and **2** consist of dinuclear Cu(II) units and μ_3-hydroxy-bridged tetranuclear Cu(II) units, respectively, their bond valence sums (BVS) calculations were performed in order to get the actual oxidation states of copper ions,[27] BVS calculations show the oxidation state of copper ions in complex **1** is 2.085, while the oxidation states of Cu(1) and Cu(2) in complex **2** are 2.038 and 2.158, respectively, suggesting the oxidation states of copper ions in complexes **1** and **2** are 2 (Table S3 and S4), which is consistent with the experimental results.

Magnetic property

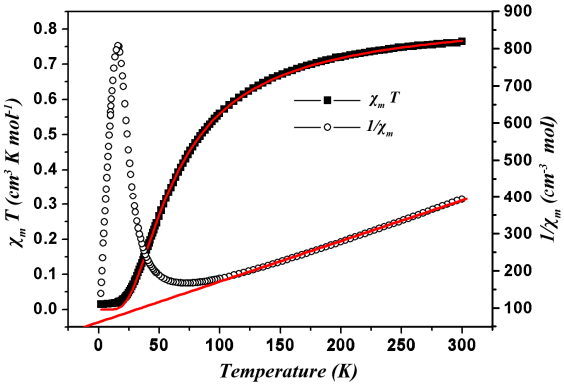

Figure 7 Temperature dependence of χ_mT and χ_m^{-1} for **1**, red solid lines represent the best theoretical fit.

The temperature-dependent magnetic susceptibilities of complexes **1** and **2** were measured under a 1000 Oe external filed at 2-300 K. The plots of χ_mT and χ_m^{-1} versus T in **1** are shown in Figure 7. χ_mT value at 2-18 K is 0.01 cm^3 K mol^{-1}. When temperature is increased, χ_mT value sharply rises to 0.56 cm^3 K mol^{-1} at 100 K, and then smoothly increases to 0.76 cm^3 K mol^{-1} at 300 K, which is close to that expected for two magnetically isolated S = 1/2 spin carriers (0.75 cm^3 mol^{-1} K). Such magnetic behavior indicates that there is an antiferromagnetic interaction in **1**. The reciprocal value of magnetic susceptibility follows Curie-Weiss law before 100 K with Curie constant C = 0.91 cm^3 K mol^{-1} and Weiss constant θ = –55.92 K. Notably, Cu(II)···Cu(II) distance in the dinuclear Cu(II)-carboxylate unit is 2.854 Å, and the smallest intercluster Cu(II)···Cu(II) separations bridged by HO-ip and bmib ligands are 9.199 and 13.499 Å, respectively. Therefore, the magnetic exchange pathways mediated by MeO-ip and BIMB ligands can be neglected, and the magnetic data can be analyzed by using Bleaney-Bowers equation derived from spin Heisenberg Hamiltonian $\hat{H} = -J\hat{S}_1\hat{S}_2$ with local spin S = 1/2. The results of the best fit are g = 2.135 ± 0.002, J = –19.68 cm^{-1}, and the agreement factor is R = 8 x 10^{-5}. The negative J value indicates the existence of an antiferromagnetic interaction, which is common for the coordination polymers consisting of dinuclear Cu(II)-carboxylate units.[25,26]

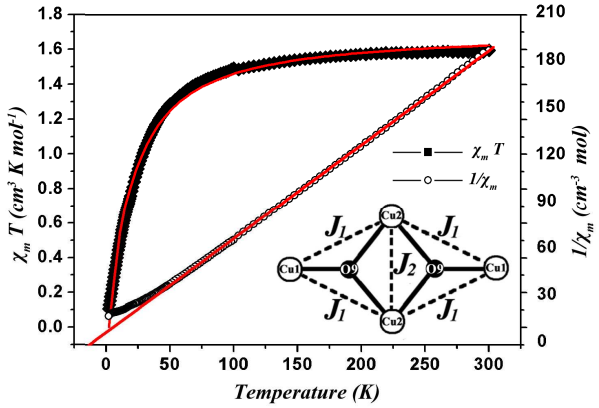

Figure 8 Temperature dependence of χ_mT and χ_m^{-1}, and magnetic exchange pathway of tetranuclear Cu(II) unit in **2**, red solid lines represent the best theoretical fit.

The temperature-dependent magnetic susceptibility data for **2** are shown in Figure 8, χ_mT at 300 K is 1.63 cm^3 K mol^{-1}, which is slightly larger than that expected for four magnetically isolated S = 1/2 spin carriers (0.15 cm^3 mol^{-1} K). Upon cooling, χ_mT decreases slowly to 1.29 cm^3 K mol^{-1} at 50 K, and then goes down sharply to a minimum value of 0.11 cm^3 K mol^{-1} at 2 K. The reciprocal value of magnetic susceptibility obeys Curie-Weiss law above 50 K. Curie constant and Weiss constant are 1.67 cm^3 K mol^{-1} and –13.32 K, respectively. The negative Weiss constant suggests the existence of antiferromagnetic interaction in complex **2**. It should be mentioned that tetranuclear Cu(II) units are well separated by MeO-ip and bmib, the closest Cu(II)···Cu(II) distance between the adjacent teternuclear unit is 8.277 Å. As a result, the tetranuclear unit may be assumed to make up the basic magnetic unit of complex **2**. In the tetranuclear Cu(II) unit, Cu1···Cu1A distance of 5.969 Å is much longer than μ_3-OH-bridged Cu(II)···Cu(II) distances from 3.046 to 3.450 Å, the magnetic exchange between Cu1 and Cu1A may be neglected, and each of these interactions is mediated by single hydroxide bridge along the long axis of the tetranuclear unit. The magnetic exchange pathways are shown in insertion of Figure 10.[28] The best fit results are J_1 = –7.96 cm^{-1} and J_2 = –10.61 cm^{-1}, no temperature-independent paramagnetism was observed, and the agreement factor R = 1.2×10^{-4}. The negative J values show that **2** has an antiferromagnetic interaction in the tetranuclear Cu(II) unit.

CONCLUSIONS

Six Cu(II) coordination polymers have been constructed using 5-substituted isophthalates and rigid bis(2-methylimidazolyl) ligands, 5-positioned substituents of isophthalate derivatives, such as HO-, MeO-, EtO-, PrO- and BnO-, are not involved in coordination with Cu(II), but they impose important effects on structures and properties of the coordination polymers. bmib in complexes **1**-**6** adopts an *anti* conformation, and bridges two Cu(II) ions. To our best knowledge, this is the first report of metal-organic coordination polymers based on bmib. Complex **1** is a two-fold interpenetrating 3-D network consisting of dinuclear Cu(II)-carboxylate units, the directional hydrogen bonds between hydroxy and carboxylate oxygen atoms are probably responsible for the formation of two-fold interpenetrating framework. The replacement of hydroxy of HO-ip by methoxyl group generates a 3-D network consisting of tetranuclear Cu(II)-carboxylate units and a 2-D layer. The use of EtO-ip gives rise to a 2-D supramolecular network containing pillared-bichain structure, while bulkier PrO-ip and BnO-ip result in the formation of 2-D layers. To our knowledge, the pillared-bichain structure of complex **4** is unprecedented in Cu(II) coordination polymers hitherto. The dinuclear and tetranuclear Cu(II) units in **1** and **2** are well separated, their magnetic analyses show the existence of antiferromagnetic interaction. In summary, this study has demonstrated that the steric and electric characters of 5-positioned coordination-inert substitutents of isophathlate derivatives and the directional hydrogen bonds play important roles in the construction of metal-organic coordination polymers, the combinational use of hydroxy-substituted 5-hydroxyisophthalates and rigid bis(2-methylimidazolyl) ligands is a useful route to generate the coordination polymers with new structures and performances. Further study of the coordination polymers based on 5-substituted isophthalates and other rigid bis(imidazolyl) ligands is on progress.

ACKNOWLEDGMENTS

This work was supported by the National Natural Science Foundation of China (21401195), the Provincial Education Department of Fujian (JA12070) and the Program for Innovative Research Team in Science and Technology in Fujian Province University (IRTSTFJ).

Notes and references

[a]*College of Materials Science and Engineering, Fujian Normal University, Fuzhou, Fujian, 350007, China.*
[b]*State Key Laboratory of Structural Chemistry, Fujian Institute of Research on the Structure of Matter, Chinese Academy of Sciences, Fuzhou, Fujian, 350002, China. E-mail: ruihu@fjirsm.ac.cn*

† Electronic Supplementary Information (ESI) available: [The additional Figures, Selected bond lengths and bond angles, TGA curves, the simulated and experimental PXRD patterns in complexes **1**-**6**]. See DOI: 10.1039/b000000x/

1 (a) C. R. Murdock, B. C. Hughes, Z. Lu and D. M.Jenkins, *Coord. Chem. Rev.,* 2014, **119,** 258; (b) E. Coronado and G. Minguez Espallargas, *Chem. Soc. Rev.,* 2013, **42**, 1525; (c) S. Mukherjee and P. S. Mukherjee, *Acc. Chem. Res.,* 2013, **46**, 2556.

2 (a) Y. S. Bae and R. Q. Snurr, *Angew. Chem., Int., Ed.* 2011, **50**, 11586; (b) C. Wang, D. Liu and W. J. Lin, *Am. Chem. Soc.,* 2013, **135**, 13222; (c) X. X. Li, H. Y. Xu, F. Z. Kong and R. H. Wang, *Angew Chem., Int. Ed.,* 2013, **52**, 13769; (d) B. Y. Li, Y. M. Zhang, D. X. Ma, T. L. Ma, Z. Shi and S. Q. Ma, *J. Am. Chem. Soc.,* 2014, **136**, 1202.

3 (a) J. Q. Liu, Y. S. Huang, Y. Y. Zhao and Z. B. Jia, *Cryst. Growth Des.,* 2011, **11**, 569; (b) Z. Yan, M. Li, H. L. Gao, X. C. Huang and D. Li, *Chem. Commun.,* 2012, **48**, 3960; (c) H. X. Zhao, X. X. Li, J. Y. Wang, L. Y. Li and R. H. Wang, *ChemPlusChem.,* 2013, **78**, 1491; (d) J. Gascon, A. Corma, F. Kapteijn, Llabres and F. X. Xamena, *ACS Catal.,* 2014, **4**, 361.

4 (a) S. Jin, W. Chen and H. Qiu, *Cryst. Growth Des.,* 2007, **7**, 2071; (b) J. Huang, P. Y. Liu, H. Zhu, S. S. Bao, L. M. Zheng and J. Ma, *ChemPlusChem.,* 2012, **77**, 1087; (c) Q. Zhang, H. Zhang, S. Zeng, D. Sun and C. Zhang, *Chem. Asian J.*, 2013, **8**, 1985.

5 (a) Y. Cui, B. Chen and G. Qian, *Coord. Chem. Rev.,* 2014, **273**, 76; (b) Y. Liu, N. Li, L. Li, H. L. Guo, X. F. Wang and Z. X. Li, *CrystEngComm,* 2012**, 14**, 2080; (c) X. Zhang, G. C. Ma, F. Z. Kong, Z. Y. Yu and R. H. Wang, *Inorg. Chem. Commun.,* 2012, **22**, 44.

6 (a) R. Heck, J. Bacsa, J. E. Warren, M. J. Rosseinsky and D. Bradshaw, *CrystEngComm*, 2008, **10**, 1687; (b) X. Zhao, H. He, T. Hu, F. Dai and D. Sun, *Inorg. Chem*., 2009, **48**, 8057; (c) Q. Chu, Z. Su, J. Fan, T. Okamura, G. C. Lv, G. X. Liu, W. Y. Sun and N. Ueyama, *Cryst. Growth Des.,* 2011, **11**, 3885; (d) Q. Yan, Y. Lin, P. Wu, L. Zhao, L. Cao, L. Peng, C. Kong and L. Chen, *ChemPlusChem.,* 2013, **78**, 86.

7 (a) X. Z. Song, S. Y. Song, M. Zhu, Z. M. Hao, X. Meng, S. N. Zhao and H. J. Zhang, *Dalton Trans.,* 2013, **42**, 13231; (b) Z. Zhang, J. F. Ma, Y. Y. Liu, W. Q. Kan and J. Yang, *Cryst. Growth Des.,* 2013, **13**, 4338; (c) Q. Chu, Z. Su, J. Fan, T. A. Okamura, G. C. Lv, G. X. Liu, W. Y. Sun and N. Ueyama, *Cryst. Growth Des.,* 2011, **11**, 3885.

8 (a) S. Q. Ma, D. F. Sun, D. Q. Yuan, X. S. Wang and H. C. Zhou, *J. Am. Chem. Soc.,* 2009, **131**, 6445; (b) D. Zhao, D. J. Timmons, D. Yuan and H. C. Zhou, *Acc. Chem. Res.* 2011, **44**, 123; (c) Y. Yan, S. Yang, A. J. Blake and M. Schroder, *Acc. Chem. Res.* 2014, **47**, 296.

9 (a) L. Pan, B. Parker, X. Y. Huang, D. H. Oison, J. Y. Lee and J. Li, *J. Am. Chem. Soc.,* 2006, **128**, 4180; (b) L. F. Ma, L. Y. Wang, Y. Y. Wang, R. B. Stuart, J. G. Wang, *Inorg. Chem*., 2009, **48**, 915; (c) D. Braga, S. D'Agostino and F. Grepioni, *CrystEngComm,* 2011, **13**, 1366; (d) X. H. Chang, L. F. Ma, G. Hui, L. Y. Wang, *Cryst. Growth Des.,* 2012, **12**, 3638; (e) H. J. Cheng, H. X. Li, Z. G. Ren, C. N. Lü, J. Shi and J. P. Lang, *CrystEngComm,* 2012, **14**, 6064.

10 (a) Q. F. Zhang, A. J. Geng, H. N. Zhang, F. L. Hu, Z. H. Lu, D. Z. Sun, X. L. Wei and C. L. Ma, *Chem. Eur. J.,* 2014, **20**, 4885; (b) J. H. Jia, S. A. Harprit, J. Alexander, N. R. Blake, Champness, H. Peter and M. Schröder, *Dalton Trans.,* 2011, **40**, 12342; (c) G. H. Wang, Y. Q. Lei, N. Wang, R. L. He, H. Q. Jia, N. H. Hu and J. W. Xu, *Cryst. Growth Des.,* 2010, **10**, 534; (d) M. H. Zeng, H. H. Zou, S. Hu, Y. L. Zhou, M. Du and H. L. Sun, *Cryst. Growth Des.,* 2009, **9**, 4239.

11 (a) F. E. Jarrod, W. Lukasz, R. H. Matthew, B. Till, Ch. K. Victor and E. Mohamed, *J. Am. Chem. Soc.,* 2011, **133**, 17532; (b) Q. Zhang, A. Geng, H. Zhang, F. Hu, Z. H. Lu, D. Sun, X. Wei and C. Ma, *Chem. Eur. J.,* 2014, **20**, 4885; (c) I. Mihalcea, N. Henry and T. Loiseau, *Eur. J. Inorg. Chem.,* 2014, 1322; (d) S. Sengupta, S. Ganguly, A. Goswami, P. K. Sukul and R. Mondal, *CrystEngCom.,* 2013, **15**, 8353; (e) T. Panda, P. Pachfule and R. Banerjee, *Chem. Commun.,* 2011, **47**, 7674.

12 H. N. Wang, X. Meng, G. S. Yang, X. L. Wang, K. Z. Shao, Z. M. Su and C. G. Wang, *Chem. Commun.,* 2011, **47**, 7128.

13 D. Zhao, S. W. Tan, D. Q. Yuan, W. G. Lu, H. R. Yohannes, H. L. Jiang, L. Q. Wang, and H. C. Zhou, *Adv. Mater*., 2011, **23**, 90.

14 J. J. Perry, G. J. McManus and M. J. Zaworotko, *Chem. Commun*., 2004, 2534.

15 (a) X. J. Li, Y. Z. Cai, Z. L. Fang, L. J. Wu, B. Wei and S. Lin, *Cryst. Growth Des.,* 2011, **11**, 4517; (b) X. J. Li, X. Y. Wang, S. Gao and R. Cao, *Inorg. Chem.,* 2006, **45**, 1508

16 (a) X. J. Li, Z. J. Yu, T. N. Guan, X. X. Li, G. C. Ma and X. F. Guo, *Cryst. Growth Des*., 2015, **15**, 278; (b) H. Abourahma, J. B. Bodwell, Lu, J. J.; B. Moulton, I. R. Pottie, R. B. Walsh and M. J. Zaworotko, *Cryst.Growth Des.* 2003, **3**, 513; (c) M. M. Zhang and F. Guo, *Synth. React. Inorg., Met.-Org., Nano-Met. Chem.* 2013, **43**, 1040.

17 (a) L. F. Ma, X. Q. Li, L. Y. Wang and H. W. Hou *CrystEngComm,* 2011, **13**, 4625; (b) K. Jiang, L. F. Ma, X. Y. Sun and L.Y. Wang, *CrystEngComm*, 2011, **13**, 330.

18 (a) Y. Qi, F. Luo, S. R. Batten, Y. X. Che and J. M. Zheng, *Cryst. Growth Des.,* 2008, **8**, 2806; (b) J. H. Qin, L. F. Ma, Y. Hu and L. Y. Wang, *CrystEngComm,* 2012, **14**, 2891.

19 (a) K. Y. Zou, J. L. Zhao, C. Liu, Z. Wang and Z. X. Li, *Eur. J. Inorg. Chem*., 2013, 293; (b) Q. X. Yang, X. Q. Chen, J. H. Cui, J. S. Hu, M. D. Zhang, L. Qin, G. F. Wang, Q. Y. Lu and H. G. Zheng, *Cryst. Growth Des.,* 2012, **12**, 4072; (c) H. Y. Zang, D. Y. Du, S. Y. Li, Y. Q. Lan, G. S. Yang, L. K. Yan, K. Z. Shao and Z. M. Su, *J. Solid State Chem.,* 2011, **184**, 1141; (d) Z. X. Li, T. L. Hu, H. Ma, Y. F. Zeng, C. J. Li, M. L. Tong and X. H. Bu, *Cryst. Growth Des*., 2010, **10**, 1138.

20 (a) Y. Qi, Y. X. Che and J. M. Zheng, *Cryst. Growth Des.,* 2008, **8**, 3602; (b) L. Zhang, Y. L. Yao, Y. X. Che and J. M. Zheng, *Cryst. Growth Des*., 2010, **10**, 528; (c) Y. Liu, Y. Qi, Y. Y. Lv, Y. X. Che and J. M. Zheng, *Cryst. Growth Des.,* 2009, **9**, 4797; (d) Y. Xu, P. K. Chen, X. X. Che and J. M. Zheng, *Eur. J. Inorg. Chem.,* 2010, 5478; (e) Z. X. Li, X. Chu, G. H. Cui, Y. Liu, L. Li and G. L. Xue, *CrystEngComm,* 2011, **13**, 1984.

21 (a) L. Chen, G. J. Xu, K. Z. Shao, Y. H. Zhao, G. S. Yang, Y. Q. Lan, X. L. Wang, H. B. Xu and Z. M. Su, *CrystEngComm,* 2010, **12**, 2157; (b) M. S. Chen, W. J. Hua, Y. Song, P. Wang, W. Y. Sun, C. Y. Zhang, G. X. Zeng and S. H. Li, *Inorg. Chim. Acta.,* 2012, **387**, 137; (c) L. Chen, K. Z. Shao, G. Yuan, G. S. Yang, H. Y. Zang, G. J. Xu, X. L. Wang and Z. M. Su, *Z. Anorg. Allg. Chem.,* 2011, **637**, 1414.

22 (a) C. Chen, J. K. Sun, W. Li, C. N. Chen and J. Zhang, *Chem. Commun*., 2011, **47** , 6683; (b) L. F. Ma, B. Liu, L. Y. Wang, C. P. Li and M. Du, *Dalton Trans*., 2010, **39**, 2301; (c) Y. Jeon, S. Cheon, S. Cho, K.Y. Lee, T. H. Kim and J. Kim, *Cryst. Growth Des.,* 2014, **14**, 2105.

23 (a) M. Bhattachary, A. G. Samuelson and P. K. Das, *J. Phys. Chem.*, 2007, **111**, 7122; (b) A. Z. Samuel and S. Ramakrishnan, *Macromolecules,* 2012, **45**, 2348.

24 (a) Sheldrick, G. M. SHELXS97; Program for Crystal Structure Solution; University of Göttingen: Göttingen, Germany, **1997**; (b) Sheldrick, G. M. SHELXL97; Program for Crystal Structure Refinement; University of Göttingen: Göttingen, Germany, **1997**.

25 X. J. Li, T. N. Guan, X. F. Guo, X. X. Li and Z. J. Yu, *Eur. J. Inorg. Chem.,* 2014**,** 2307.

26 (a) S. L. Xiang, J. Huang, L. Li, J. Y. Zhang, L. Jiang, X. J. Kuang and C. Y. Su, *Inorg. Chem.,* 2011, **50**, 1743; (b) Y. Cai, Y. D. Zhang, Y. G. Huang, R. M. Seth and S. W. Krista, *Cryst. Growth Des.*, 2012**, 12**, 3709.

27 (a) N. E. Brese and M. O'Keeffe, *Acta Cryst.*, 1991, **B47**, 192; (b) I. D. Brown, 2002, The Chemical Bond in Inorganic Chemistry: The Bond Valence Model. Oxford University Press.

28 A. Mondal, Y. Li, M. A. Khan, J. H. Jr. Ross and R. P. Houser, *Inorg. Chem.,* 2004, **43**, 7075.

Graphic Abstract

Effects of Hydroxy Substitutents on Cu(II) Coordination Polymers Based on 5-Hydroxyisophthalate Derivatives and 1,4-Bis(2-methylimidazol-1-yl)benzene

Six Cu(II) coordination polymers based on 5-Hydroxyisophthalate and hydroxy-substituted 5-alkyloxyisophthalate have been presented. The hydroxyl- and alkyloxy- substituents are not involved in coordination with Cu(II), but their steric and electric characters as well as the directional hydrogen bonds impose important effects on the structures and properties of the coordination polymers.